Central European Journal of Energetic Materials
ISSN 1733-7178; e-ISSN 2353-1843

Cent. Eur. J. Energ. Mater. 2018, *15*(1): 115-130; DOI: 10.22211/cejem/78089

Analysis of the Thermal Behaviour of CL-20, Potassium Perchlorate, Lithium Perchlorate and Their Admixtures by DSC and TG

Jing-yuan Zhang, Xue-yong Guo,* Qing-jie Jiao, Hong-lei Zhang, Hang Li

State Key Laboratory of Explosion Science and Technology, Beijing Institute of Technology, Beijing 100081, China
**E-mail: wo525291980@163.com*

Abstract: The thermal decomposition characteristics of CL-20, potassium perchlorate (KP), lithium perchlorate (LP), a CL-20/KP mixture, and a CL-20/LP mixture were studied using thermogravimetry-differential scanning calorimetry (TG-DSC). The DSC curves for KP exhibited three endothermic peaks and one exothermic peak. The first two endothermic peaks correspond to the rhombic-cubic transition and the fusion of KP, respectively, the third indicates the fusion of KCl, while the exothermic peak is attributed to the decomposition of KP. The DSC curves obtained from LP showed four endothermic peaks and one exothermic peak. The first two endothermic peaks indicate the loss of adsorbed water and water of crystallization, while the third and fourth are associated with the fusion of LP and LiCl, respectively; the exothermic peak is due to the decomposition of LP. The presence of KP had little effect on the thermal decomposition of CL-20 while the addition of LP increased the temperature at which CL-20 exhibits an exothermic peak. In addition, the thermal decomposition of LP appeared to be catalyzed by the presence of CL-20.

Keywords: CL-20, potassium perchlorate, lithium perchlorate, thermal stability, phase transition

1 Introduction

CL-20 is one of the most important high energy and high density compounds, and exhibits 14-20% higher performance than HMX-based plastic bonded

explosives (PBXs) [1-4]. Because it also generates superior detonation velocities and pressures, CL-20 is a suitable candidate for replacing HMX in explosive formulations [5-9]. Under ambient conditions, CL-20 has four different polymorphs, α, β, γ and ε. The ε-phase has the highest density (2.04 $g \cdot cm^{-3}$) and the greatest stability, and so it is the preferred phase for high energy applications [10-15].

Potassium, lithium and ammonium perchlorate (KP, LP and AP) are the oxidizers most commonly used in propellants, pyrotechnics, and PBXs, and the thermal behaviour of these oxidizers will have a significant effect on the properties of the resulting formulations. Many studies have researched the thermal decomposition of CL-20 and AP on their own and in combination [16-19]. Turcotte *et al*. [20] examined the thermal decomposition of CL-20 at heating rates of 1 $°C \cdot min^{-1}$, 2 $°C \cdot min^{-1}$, 5 $°C \cdot min^{-1}$, and 10 $°C \cdot min^{-1}$, while the activation energy for CL-20 decomposition was determined by the Kissinger method to be 207 ±18 $kJ \cdot mol^{-1}$; they also determined that CL-20 loses approximately 85% of its initial mass during the decomposition. Xiang *et al.* [21] studied the thermal behaviour of CL-20 by differential scanning calorimetry-thermogravimetry-Fourier transform infrared spectroscopy (DSC-TG-FT-IR), and showed that the apparent activation energy values for CL-20 as calculated by the Kissinger and Ozawa methods were 194.8 $kJ \cdot mol^{-1}$ and 193.6 $kJ \cdot mol^{-1}$, respectively. However, to the best of our knowledge, the thermal decomposition and reaction kinetics of the CL-20/KP and CL-20/LP mixtures have never been investigated. Because the use of KP and LP in CL-20-based PBXs will affect the performance of these explosives, the present work examined the thermal decomposition of CL-20/KP and CL-20/LP by TG-DSC.

2 Experimental

2.1 Materials and characterization

ε-CL-20, obtained from the Qingyang Chemical Industry Corporation (Liaoning Province, China), was recrystallized using ethyl acetate as the solvent and trichloromethane as the anti-solvent prior to the experimental trials. The resulting particle sizes were in the range of 100-300 μm, with a mean size of 120 μm. The FT-IR spectrum and X-ray diffraction (XRD) pattern of the CL-20 obtained from this recrystallization are shown in Figures 1 and 2. The characteristic FT-IR peaks in the region of 1200-700 cm^{-1} are consistent with the ε-CL-20 spectra in the literature [22, 23]. The XRD pattern is also in agreement, confirming that the sample was composed of ε-CL-20.

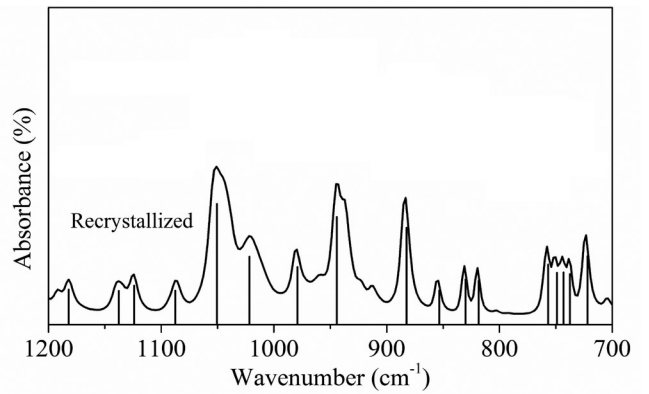

Figure 1. FT-IR spectrum of recrystallized CL-20

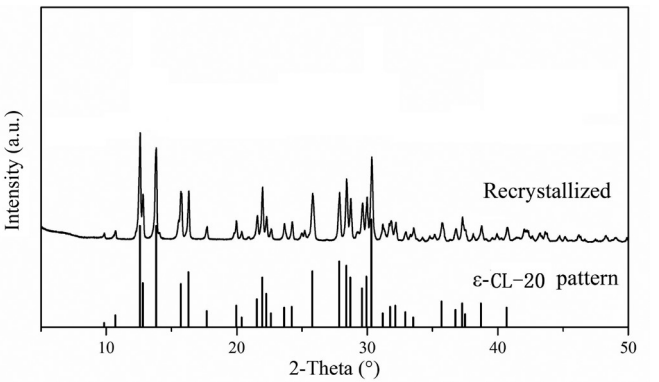

Figure 2. XRD pattern of recrystallized CL-20

The KP used in this work was obtained from the Aladdin Industrial Corporation and was analytical grade with a particle size range of 50-150 μm. The LP (Shanghai China Lithium Industrial Co., Ltd.) was technical grade with a particle size range of 150-500 μm. Combinations of ε-CL-20 and powdered KP or LP were prepared by mixing the two components in a mixer for 40 min at a 1:1 ε-CL-20 to KP or LP mass ratio.

2.2 Thermal analysis

The TG-DSC analyses of the samples were performed with a Netzsch STA449-F3 (Germany) simultaneous thermal analyzer at different heating rates (5 $K \cdot min^{-1}$, 10 $K \cdot min^{-1}$, 15 $K \cdot min^{-1}$ and 20 $K \cdot min^{-1}$) under a 30 $mL \cdot min^{-1}$ flow of argon. The Kissinger and Flynn-Wall-Ozawa methods were used to obtain the kinetic parameters based on the non-isothermal data.

3 Results and Discussion

3.1 Thermal behaviour of the individual components

3.1.1 CL-20

The TG and DSC curves summarizing the thermal behaviour of CL-20 when heated from 30-400 °C at 5 K·min^{-1}, 10 K·min^{-1}, 15 K·min^{-1} or 20 K·min^{-1} are shown in Figure 3. From Figure 3b, it may be seen that the decomposition of CL-20 is a "one-step" process, which is not consistent with the conclusion of Turcotte [20] that the mass loss curve indicates a "two-step" process. This discrepancy may be due to the variations in the particle size and size distribution of the CL-20. The TG curves also showed that CL-20 loses 85 ±5% of its initial mass during decomposition. The DSC curve exhibited a single exothermic peak at approximately 250 °C, corresponding to the mass loss step in the TG curve. Table 1 summarizes the temperatures at which CL-20 undergoes thermal decomposition at various heating rates. Based on the non-isothermal TG-DTG analysis of CL-20 at these four heating rates, the associated decomposition kinetic parameters were calculated using the Kissinger and Flynn-Wall-Ozawa methods (based on Equations 1 and 2 below) and these are also listed in Table 1.

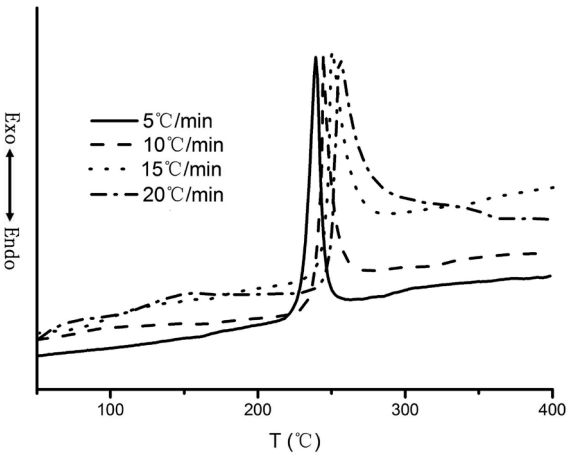

(a) DSC curves

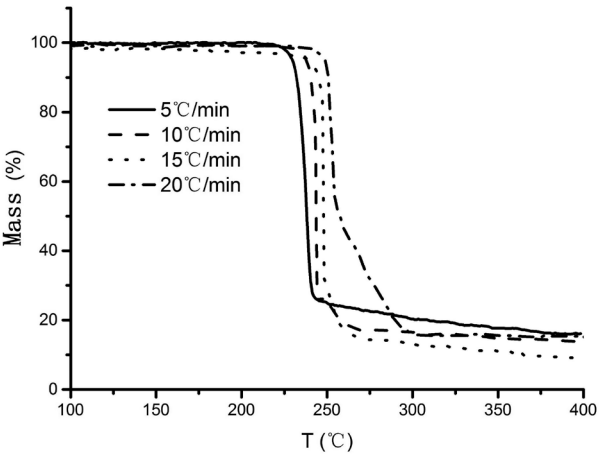

(b) TG curves

Figure 3. DSC and TG curves for CL-20

Kissinger method:

$$\ln\left[\frac{\beta}{T_p^{\,2}}\right] = \ln\left(\frac{A_k R}{E_k}\right) - \frac{E_k}{RT_p} \tag{1}$$

Flynn-Wall-Ozawa method:

$$\lg \beta = \lg\left(\frac{AE_O}{RG(\alpha)}\right) - 2.315 - 0.4567\frac{E_O}{RT} \tag{2}$$

In the above equations, β is the heating rate in $K \cdot min^{-1}$, T_p is the peak temperature of the DTG curve at β (in K), A and A_k are the pre-exponential factors, E_k and E_O are the apparent activation energy values determined by the Kissinger and Ozawa methods, respectively ($J \cdot mol^{-1}$), R is the ideal gas constant (8.314 $J \cdot mol^{-1} \cdot K^{-1}$), T is the absolute temperature and the temperature of the DTG curve, α is the conversion degree (the mass ratio of the amount of material reacted to the initial amount), and $G(\alpha)$ is the integral mechanism function.

Equation 1 predicts a linear relationship between $\ln(\beta/T_p^2)$ and $1/T_p$, and suggests that the activation energy (E_k) and the pre-exponential factors (A_k) can be calculated from the slope and intercept. In the case of the Ozawa method, the effect of the value of α on T will remain approximately constant at different

heating rates, and E_O can be calculated from the linear relationship between lg(β) and 1/*T*.

The values of the activation energy were consistent with those reported by Geetha *et al*. [3] and Turcotte *et al*. [20], who have carried out a similar study using heating rates from 10 K·min^{-1} to 25 K·min^{-1} (E_k = 199.45 kJ·mol^{-1}) and 1 K·min^{-1} to 10 K·min^{-1} (E_k = 207 ±18 kJ·mol^{-1}), respectively.

Table 1. Temperatures and kinetic parameters for the thermal decomposition of CL-20 at various heating rates

Heating rate [K·min^{-1}]	DSC peaks T_p [°C]	DTG peaks T_p [°C]	E_k [kJ·mol^{-1}]	lg(A_k/s^{-1})	r_k	E_O [kJ·mol^{-1}]	r_O
5	239.4	238.1	198.7	18.2	0.993	197.1	0.993
10	245.2	243.9					
15	251.2	249.9					
20	254.2	252.5					

3.1.2 KP

The DSC and TG data obtained from KP heated from 30 °C to 900 °C at rates of 5 K·min^{-1}, 10 K·min^{-1}, 15 K·min^{-1} and 20 K·min^{-1} are shown in Figure 4. The DSC plot generated at 10 K·min^{-1} exhibited three endothermic peaks at 302.9 °C, 476.8 °C and 764.1 °C, and one exothermic peak at 490.8 °C. The first two endothermic peaks are attributed to the phase transition and fusion of KP, while the third peak is due to the fusion of KCl, and the exothermic peak represents the decomposition of KP. The quantities of the endothermic and exothermic peaks in the DSC results obtained during the present study are in agreement with data published in the literature [24]. Table 2 summarizes the thermal decomposition process of KP at various heating rates. As KCl melts and volatizes, the TG curves show that the KP loses approximately 90% of its initial mass. Based on the non-isothermal TG-DTG data obtained from KP at the four heating rates, the parameters for the decomposition kinetics of KP were calculated by the Kissinger and Flynn-Wall-Ozawa methods and these values are also provided in Table 2.

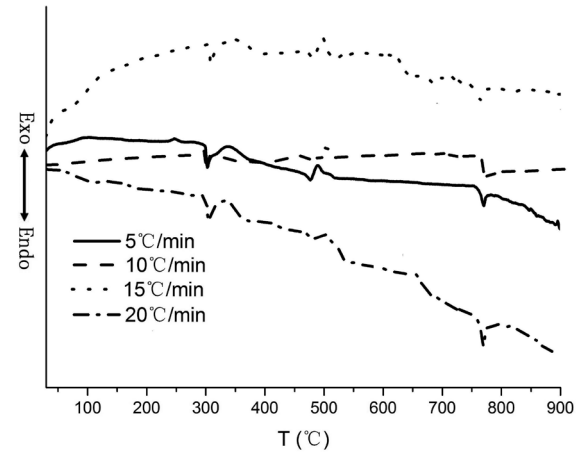

(a) DSC curves

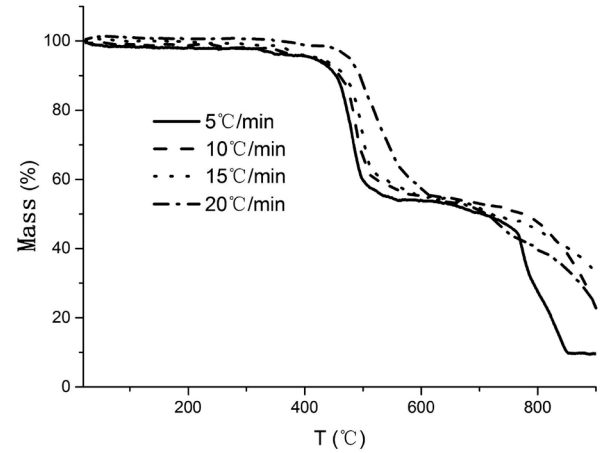

(b) TG curves

Figure 4. DSC and TG curves for KP

Table 2. Temperatures and kinetic parameters for the thermal decomposition of KP at various heating rates

Heating rate [K·min^{-1}]	DSC peaks T_p [°C]	DTG peaks T_p [°C]	E_k [kJ·mol^{-1}]	$\lg(A_k/s^{-1})$	r_k	E_O [kJ·mol^{-1}]	r_O
5	480.5	474.8	218.5	12.86	0.997	219.8	0.997
10	490.8	487.9					
15	500.1	498.6					
20	504.3	502.8					

3.1.3 LP

The DSC and TG curves generated by LP at heating rates of 5 K·min^{-1}, 10 K·min^{-1}, 15 K·min^{-1} and 20 K·min^{-1} are shown in Figure 5. Because LP tends to absorb moisture from the air and form a crystalline hydrate ($LiClO_4$•$3H_2O$) [25], the DSC curve obtained at 10 K·min^{-1}, exhibited two endothermic peaks at 91.6 °C and 149.1 °C, while the TG data showed two mass loss steps, corresponding to the loss of adsorbed water and water of crystallization. In this same DSC curve, LP showed another endothermic peak at 247.8 °C, although there was no corresponding mass loss in the TG data, meaning that the peak is related to a fusion process. The DSC plot acquired at 10 K·min^{-1} also had one exothermic peak at 508 °C and the TG curve indicated a mass loss at this temperature, such that the exothermic peak suggests decomposition of LP. A fourth endothermic peak in the DSC curve corresponds to the fusion of LiCl. These results are in agreement with previously reported data [26]. The temperatures associated with the thermal decomposition of LP and the decomposition kinetic parameters were calculated by the Kissinger and Flynn-Wall-Ozawa methods and the resulting values are summarized in Table 3.

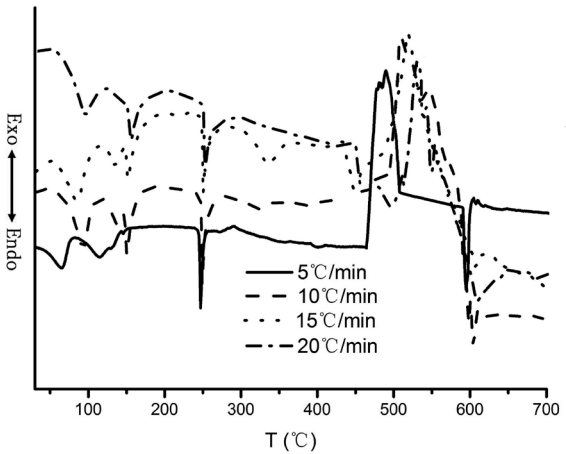

(a) DSC curves

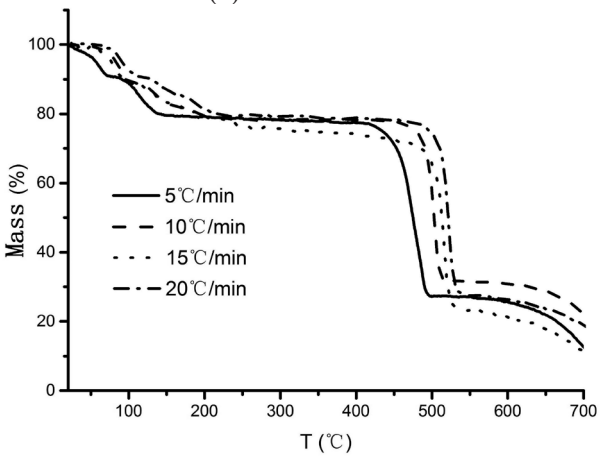

(b) TG curves

Figure 5. DSC and TG curves for LP

Table 3. Temperatures and kinetic parameters for the thermal decomposition of LP at various heating rates

Heating rate [K·min^{-1}]	DSC peaks T_p [°C]	DTG peaks T_p [°C]	E_k [kJ·mol^{-1}]	$\lg(A_k/s^{-1})$	r_k	E_O [kJ·mol^{-1}]	r_O
5	489.5	486.5	191.4	10.68	0.998	194.3	0.998
10	508.0	502.8					
15	516.6	514.5					
20	527.8	519.6					

3.2 Thermal behaviour of mixtures

3.2.1 Thermal behaviour of CL-20/KP mixtures

Figure 6 shows the DSC and TG curves for a CL-20/KP mixture (1:1 by mass). The TG data exhibited three mass loss steps, the first of which is attributed to the thermal decomposition of CL-20 because the peak temperature is almost equal to that obtained from pure CL-20. The second mass loss step was caused by the decomposition of the KP. The peak temperature of this step was higher than that of pure KP, suggesting that the thermal decomposition of KP was retarded by the presence of CL-20. The third mass loss step resulted from the volatilization of KCl. The temperatures for the thermal decomposition of the CL-20/KP mixture and the decomposition kinetic parameters were calculated using the Kissinger and Flynn-Wall-Ozawa methods and are summarized in Table 4.

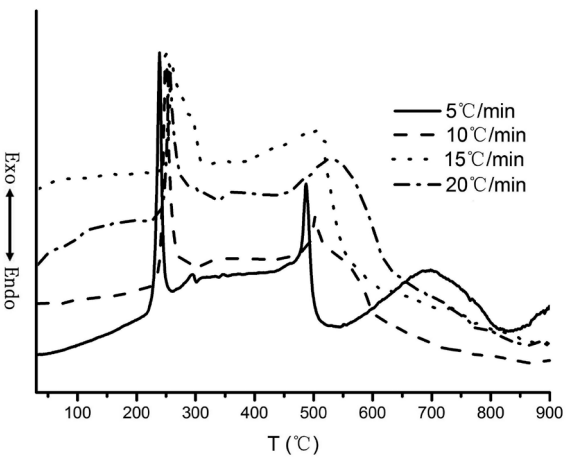

(a) DSC curves

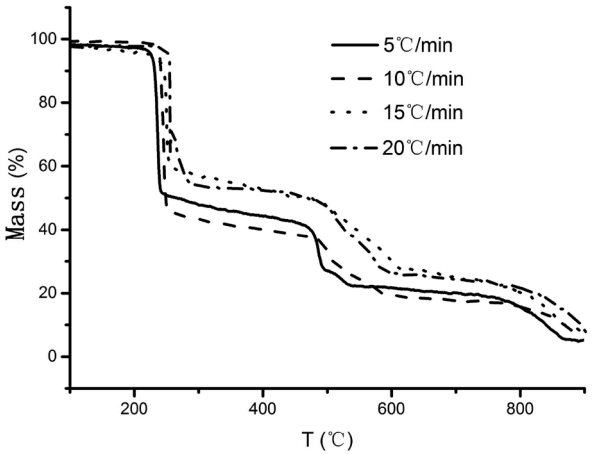

(b) TG curves

Figure 6. DSC and TG curves for CL-20/KP

Table 4. Temperatures and kinetic parameters for the initial thermal decomposition of CL-20/KP at various heating rates

Heating rate [K·min^{-1}]	DSC peaks T_p [°C]	DTG peaks T_p [°C]	E_k [kJ·mol^{-1}]	$\lg(A_k/s^{-1})$	r_k	E_O [kJ·mol^{-1}]	r_O
5	239.7	238.4	200.0	18.31	0.996	198.4	0.996
10	247.0	245.6					
15	252.2	250.9					
20	254.6	252.7					

Table 5. Temperatures and kinetic parameters for the second thermal decomposition of CL-20/KP at various heating rates

Heating rate [K·min^{-1}]	DSC peaks T_p [°C]	DTG peaks T_p [°C]	E_k [kJ·mol^{-1}]	$\lg(A_k/s^{-1})$	r_k	E_O [kJ·mol^{-1}]	r_O
5	490.8	487.4	176.4	9.598	0.999	180.0	0.999
10	507.9	505.6					
15	519.6	517.3					
20	527.3	523.8					

3.2.2 Thermal behaviour of CL-20/LP mixtures

Figure 7 presents the DSC and TG data obtained from CL-20/LP specimens. The TG curves showed that there are five mass loss steps for the CL-20/LP mixture. The LP generated two endothermic peaks at 96.6 °C and 148.6 °C in the DSC plot at 10 $K \cdot min^{-1}$, while the TG plot showed two mass loss steps at these temperatures. These two mass loss steps correspond to the loss of adsorbed water and water of crystallization. The third mass loss step for the CL-20/LP mixture is ascribed to the thermal decomposition of CL-20, although the peak temperature obtained from the mixture is higher than that of pure CL-20. This may have occurred because the melting temperature of LP is close to the decomposition temperature of CL-20 and the LP absorbs heat when melting, thus raising the decomposition temperature of the CL-20. The fourth mass loss step is ascribed to the decomposition of the LP. The peak temperature of this step is low compared to that of pure LP, suggesting that the thermal decomposition of LP is catalyzed by the presence of CL-20. The fifth mass loss step for the CL-20/LP mixture corresponds to the volatilization of LiCl. The related temperatures for the thermal decomposition of CL-20/LP and the decomposition kinetic parameters were calculated by the Kissinger and Flynn-Wall-Ozawa methods and are summarized in Table 5.

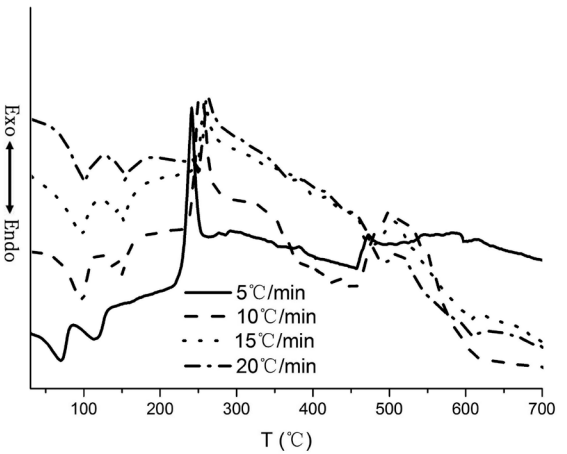

(a) DSC curves

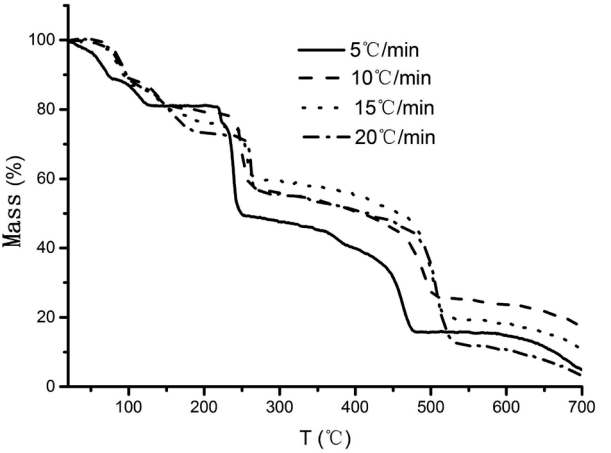

(b) TG curves

Figure 7. DSC and TG curves for CL-20/LP

Table 6. Temperatures and kinetic parameters for the initial thermal decomposition of CL-20/LP at various heating rates

Heating rate [K·min^{-1}]	DSC peaks T_p [°C]	DTG peaks T_p [°C]	E_k [kJ·mol^{-1}]	$\lg(A_k/s^{-1})$	r_k	E_O [kJ·mol^{-1}]	r_O
5	241.0	239.5	151.4	13.21	0.995	152.3	0.995
10	251.6	247.3					
15	257.1	254.5					
20	259.2	258.8					

Table 7. Temperatures and kinetic parameters for the second thermal decomposition of CL-20/LP at various heating rates

Heating rate [K·min^{-1}]	DSC peaks T_p [°C]	DTG peaks T_p [°C]	E_k [kJ·mol^{-1}]	$\lg(A_k/s^{-1})$	r_k	E_O [kJ·mol^{-1}]	r_O
5	477.1	466.8	155.2	8.4	0.998	159.6	0.999
10	495.3	487.9					
15	503.0	498.6					
20	509.9	506.2					

4 Conclusions

The thermal decomposition characteristics of CL-20, KP, LP, a CL-20/KP mixture, and a CL-20/LP mixture were studied using TG-DSC. The DSC curve for KP at 10 $K \cdot min^{-1}$ showed an endothermic peak at 302.9 °C, corresponding to a rhombic-cubic transition, and also exhibited fusion at 480 °C and decomposition at 489.3 °C. The presence of KP evidently had a minimal effect on the thermal decomposition of CL-20 in the CL-20/KP mixture because there was little change in the apparent activation energy of the CL-20 decomposition as calculated by the Kissinger method.

The DSC data for LP showed four endothermic peaks and one exothermic peak, with the first two endothermic peaks indicating the loss of adsorbed water and water of crystallization, and the third and fourth endothermic peaks corresponding to the fusion of LP and LiCl, respectively. The exothermic peak is attributed to the decomposition of LP. The presence of LP increases the exothermic peak temperature of CL-20 and the thermal decomposition of LP is evidently catalyzed by the presence of CL-20. The activation energy for CL-20 decomposition in the presence of LP is lowered by approximate 50 kJ/mol.

Acknowledgments
We would like to express our gratitude to Dr. Yalun Sun for her enthusiastic help in this work.

References

[1] Samudre, S. S.; Nair, U. R.; Gore, G. M.; Sinha, R. K.; Sikder, A. K.; Asthana, S. N. Studies on an Improved Plastic Bonded Explosive (PBX) for Shaped Charges. *Propellants Explos. Pyrotech.* **2009**, *34*(2): 145-150.

[2] Guo, X. D.; Ouyang, G.; Liu, J.; Li, Q.; Wang, L. X.; Gu, Z. M.; Li, F. S. Massive Preparation of Reduced-Sensitivity Nano CL-20 and its Characterization. *J. Energ. Mater*. **2015**, *33*(1): 24-33.

[3] Geetha, M.; Nair, U. R.; Sarwade, D. B.; Gore, G. M.; Asthana, S. N.; Singh, H. Studies on CL-20: the Most Powerful High Energy Material. *J. Therm. Anal. Calorim*. **2003**, *73*(3): 913-922.

[4] Nair, U. R.; Gore, G. M.; Sivabalan, R.; Satpute, R. S.; Asthana, S. N.; Singh, H. Studies on Polymer Coated CL-20 − the Most Powerful Explosive. *J. Poly. Mater*. **2003**, *21*(4): 377-382.

[5] Nair, U. R.; Sivabalan, R.; Gore, G. M.; Geetha, M.; Asthana, S. N.; Singh, H. Hexanitrohexaazaisowurtzitane (CL-20) and CL-20-based Formulations (Review).

Combust., Explos. Shock Waves **2005**, *41*(2): 121-132.
[6] Ordzhonikidze, O.; Pivkina, A.; Frolov, Yu.; Muravyev, N.; Monogarov, K. Comparative Study of HMX and CL-20: Thermal Analysis, Combustion and Interaction with Aluminium. *J. Therm. Anal. Calorim*. **2011**, *105*(2): 529-534.
[7] Sivabalan, R.; Gore, G. M.; Nair, U. R.; Aaikia, A.; Venugopalan, S.; Gandhe, B. R. Study on Ultrasound Assisted Precipitation of CL-20 and its Effect on Morphology and Sensitivity. *J. Hazard. Mater*. **2007**, *139*(2): 199-203.
[8] Bayat, Y.; Zeynali, V. Preparation and Characterization of Nano-CL-20 Explosive. *J. Energ. Mater*. **2011**, *29*(4): 281-291.
[9] Ghosh, M.; Venkatesan, V.; Sikder, N.; Sikder, A. K. Quantitative Analysis of α-CL-20 Polymorphic Impurity in ε-CL-20 Using Dispersive Raman Spectroscopy. *Cent. Eur. J. Energ. Mater*. **2013**, *10*(3): 419-438.
[10] Goede, P.; Latypov, N. V.; Östmark, H. Fourier Transform Raman Spectroscopy of the Four Crystallographic Phases of α, β, γ and ε 2,4,6,8,10,12-Hexanitro-2,4,6,8,10,12-hexaazatetracyclo[5.5.0.$0^{5,9}$.$0^{3,11}$]dodecane (HNIW, CL-20). *Propellants Explos. Pyrotech*. **2004**, *29*(4): 205-208.
[11] Chen, H. X.; Chen, S. S.; Li, L. J.; Jin, S. H. Quantitative Determination of ε-Phase in Polymorphic HNIW Using X-ray Diffraction Patterns. *Propellants Explos. Pyrotech*. **2008**, *33*(6): 467-471.
[12] Agrawal, J. P. Some New High Energy Materials and Their Formulations for Specialized Applications. *Propellants Explos. Pyrotech*. **2005**, *30*(5): 316-328.
[13] Elbeih, A.; Husarova, A.; Zeman, S. Path to ε-HNIW with Reduced Impact Sensitivity. *Cent. Eur. J. Energ. Mater*. **2011**, *8*(3): 173-182.
[14] Urbelis, J. H.; Swift, J. A. Solvent Effects on the Growth Morphology and Phase Purity of CL-20. *Crystal Growth & Design* **2014**, *14*(4): 1642-1649.
[15] Dorofeeva, O. V.; Suntsova, M. A. Enthalpy of Formation of CL-20. *Comput. Theor. Chem.* **2015**, *1057*(6): 54-59.
[16] Nedelko, V. V.; Chukanov, N. V.; Raevskii, A. V.; Korsounskii, B. L.; Larikova, T. S.; Kolesova, O. I. Comparative Investigation of Thermal Decomposition of Various Modifications of Hexanitrohexaazaisowurtzitane (CL-20). *Propellants Explos. Pyrotech*. **2000**, *25*(5): 255-259.
[17] Dong, L. M.; Li, X. D.; Yang, R. J. Thermal Decomposition Study of HNIW by Synchrotron Photoionization Mass Spectrometry. *Propellants Explos. Pyrotech*. **2011**, *36*(6): 493-498.
[18] Zhu, Y. L.; Wang, K. K.; Shan, M. X.; Zheng, X. D.; Jiao, Q. J.; Wang, J. S. Thermal Decomposition Kinetics of Hexanitrohexaazaisowurtzitane/Ammonium Perchlorate. *Cent. Eur. J. Energ. Mater*. **2016**, *13*(1): 149-159.
[19] Zhu, Y. L.; Shan, M. X.; Zheng, X. D.; Wang, J. S.; Jiao, Q. J. Kinetics of Thermal Decomposition of ε-Hexanitrohexaazaisowurtzitane by TG-DSC-MS-FTIR. *Korean J. Chem. Eng*. **2015**, *32*(6): 1164-1169.
[20] Turcotte, R.; Vachon, M.; Kwok, Q. S. M.; Wang, R. P.; Jones, D. E. G. Thermal Study of HNIW (CL-20). *Thermochim. Acta* **2005**, *433*(1): 105-115.
[21] Xiang, M.; Jiao, Q. J.; Zhu, Y. L.; Yu, J. Y.; Chen, L. P. Thermal Study of HNIW

(CL-20) and Mixtures Containing Aluminum Powder. *J. Therm. Anal. Calorim*. **2014**, *116*(3): 1159-1163.

[22] Hakobu, B.; Shuichi, K.; Hiroshi, M. Y. Synthesis and Sensitivity of Hexanitrohexaazaisowurtzitane (HNIW). *Propellants Explos. Pyrotech*. **1998**, *23*(6): 333-336.

[23] Jin, S. H.; Shu, Q. H.; Chen, S. S. Preparation of ε-HNIW by a One-pot Method in Concentrated Nitric Acid from Tetraacetyldiformylhexaazaisowurtzitane. *Propellants Explos. Pyrotech*. **2007**, *32*(6): 468-472.

[24] Lee, J. S.; Hsu, C. K. The DSC Studies on the Phase Transition, Decomposition and Melting of Potassium Perchlorate with Additives. *Thermochim. Acta* **2001**, *367-368*(1): 367-370.

[25] Wickleder, M. S. Crystal Structure of $LiClO_4$. *Cheminform* **2003**, *34*(44): 1466-1468.

[26] Yan, K.; Zhang, Y. W.; Wang, Y. C.; Liu, J. Z.; Zhou, J. H.; Cen, K. F. Kinetic Study of Lithium Perchlorate Decomposition Mechanism. *J. Solid Rocket Tech*. **2013**, *36*(3): 353-357.